Article

Cite This: *Biomacromolecules* 2019, 20, 2105−2114

pubs.acs.org/Biomac

Plasticized Cellulosic Films by Partial Esterification and Welding in Low-Concentration Ionic Liquid Electrolyte

Xun Niu,[†,‡] Yating Liu,[†] Alistair W. T. King,[§] Sami Hietala,[§] Hui Pan,[*,†] and Orlando J. Rojas[*,‡]

[†]Jiangsu Co-Innovation Center for Efficient Processing and Utilization of Forest Resources, College of Chemical Engineering, Nanjing Forestry University, 159# Longpan Road, Nanjing 210037, P. R. China

[‡]Department of Bioproducts and Biosystems, School of Chemical Engineering, Aalto University, PO Box 16300, FIN-00076 Aalto, Espoo, Finland

[§]Materials Chemistry, Department of Chemistry, Faculty of Science, University of Helsinki, A.I. Virtasen aukio 1, PO Box 55, FIN-00014, Finland

Supporting Information

ABSTRACT: Alternatives to petroleum-based plastics are of great significance not only from the point of view of their scientific and practical impact but to reduce the environmental footprint. Inspired by the composition and structure of wood's cell walls, we used phenolic acids to endow cellulosic fibers with new properties. The fiber dissolution and homogeneous modification were performed with a recyclable ionic liquid (IL) (tetrabutylammonium acetate ([N_{4444}][OAc]):dimethyl sulfoxide) to attain different levels of reaction activity for three phenolic acids (*p*-hydroxybenzoic acid, vanillic acid, and syringic acid). The successful autocatalytic Fischer esterification reaction was thoroughly investigated by Fourier transform infrared spectroscopy, X-ray photoelectron spectroscopy, elemental analysis, and nuclear magnetic resonance spectroscopy (^{13}C CP-MAS, diffusion-edited ^{1}H NMR and multiplicity-edited heteronuclear single quantum coherence). Control of the properties of cellulose in the dispersed state, welding, and IL plasticization were achieved during casting and recrystallization to the cellulose II crystalline allomorph. Films of cellulose carrying grafted acids were characterized with respect to properties relevant to packaging materials. Most notably, despite the low degree of esterification (DS < 0.25), the films displayed a remarkable strength (3.5 GPa), flexibility (strains up to 35%), optical transparency (>90%), and water resistance (WCA ∼ 90°). Moreover, the measured water vapor barrier was found to be similar to that of poly(lactic acid) composite films. Overall, the results contribute to the development of the next-generation green, renewable, and biodegradable films for packaging applications.

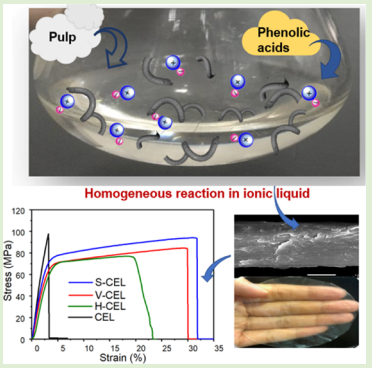

INTRODUCTION

Concerns regarding the pollution generated by plastics used for packaging have led to increased efforts to find low-cost alternatives, preferably if they display multiple properties such as sustainability, flexibility, transparency, and strength, as demanded by the given applications. It is not surprising that cellulose has attracted renewed attention, given its possibility for chemical modification and for developing features that are desirable in biomedical,[1] electronic,[2] and optical[3] applications. Cellulose can also be bestowed with adsorption and separation capabilities,[4,5] hydrophobicity,[6] and stimuli responsiveness.[7,8] However, modification methods such as esterification, silanization, and etherification are often difficult to implement and, especially, to scale up, due to the inherent use of hazardous chemicals, solvents, and release of toxic gases.[9] The abundant hydroxyl groups on the cellulosic materials engage in intermolecular and intramolecular hydrogen bondings, which result in their insolubility in common solvents and general difficultly in processing. Thus, it is desirable to process cellulose via simple, efficient, and environmentally friendly methods. In this context, the conversion of cellulose into homogeneous solutions is quite attractive and the key for this process is to find efficient, low-toxicity, chemically stable, and recyclable cellulose solvents.

Some Ionic liquids (ILs), often composed of mixed organic and inorganic anions and cations, have been investigated for fractionation of lignocellulosic materials and are able to dissolve cellulose and its derivatives.[10] Compared to conventional solvents, ILs are often considered as "green solvents" due to their low volatility and the ability of some ILs to dissolve cellulose. However, they should only be considered so if they have high chemical and thermal stability, have low toxicity, and are recyclable. The high anion basicity required to disrupt the hydrogen bonding network in crystalline cellulose introduces instability to an ionic liquid;[11] therefore, careful choice of ionic components is important.

Despite, their unique properties, the high cost of typical ILs and challenges in their recovery severely limit their use. Thus, efforts have been made to investigate co-solvents to reduce the overall cost. Dimethyl sulfoxide (DMSO), for example, has

Received: March 5, 2019
Revised: April 10, 2019
Published: April 15, 2019

DOI: 10.1021/acs.biomac.9b00325
Biomacromolecules 2019, 20, 2105−2114

been reported to improve cellulose swelling and solubility and to disrupt hydrogen bonding. Co-solvents as such may also play roles as "viscosity reducers" and enable faster mass transport of the system with little or no interaction with the given ILs.[12] Thus, there are advantages to finding mixtures with as low consistency as possible, yet with the ability still to mold or modify the properties of cellulose. ILs also allow for further chemical conversions, not possible in heterogeneous systems.

In this respect, phenolic acids having one or more phenolic hydroxyl groups on the aromatic ring can be considered as suitable biobased feedstocks for chemical modifications. They can be derived from plants (including fruits, vegetables, and mushrooms) or from lignin biodegradation.[13,14] These compounds include vanillic acid (VA), *p*-hydroxybenzoic acid (HA), and syringic acid (SA), which are attractive owing to additional beneficial properties, including antioxidant, anti-inflammatory, antitumor, and hypoglycemic activities.[15] The primary and the secondary walls of plant cells include a hierarchical assembly of cellulose microfibrils, hemicelluloses, and aromatic lignin bound together by chemical, physical, and other links,[14] all of which contribute to a flexible yet strong structure. Inspired by related principles, biomimetic materials can be developed. Recently, phenolic acids have been applied to nanoparticles[16] and polymers.[17,18] Especially, VA has been used for grafting onto chitosan to develop antioxidant activity, for instance for packaging of fish oil;[18−20] although amides, formed from reaction of chitosan with phenolic acids, are expected to form more readily on cellulose than oxoesters, this provides a motivation to consider other phenolic-grafted, biobased polymers to achieve bioactive packaging and food additives.

Typical cellulose-based packaging materials are reported to have a tensile strength of 100−300 MPa and strain of 1−10%.[21] Despite this outstanding performance, such materials and, especially their brittleness, still need improvement to become alternatives to plastics. Cellulose-based films that simultaneously display high flexibility, strength, and transparency are still to be developed, and their potential utilization as plastic remains a challenge.

Herein, inspired by the nature of plant's cell walls, we consider the mechanical and functional performance of packaging materials with regards to their intrinsic properties and interfacial adhesion. A series of cellulose esters grafted with phenolic acids (HA, VA, and SA) were prepared using a room-temperature ionic liquid system, tetrabutylammonium acetate ($[N_{4444}][OAc]$): dimethyl sulfoxide (DMSO). The phenolic acids feature a different number of methoxy groups ($-OCH_3$), 0, 1 and 2 in HA, VA, and SA, respectively. Accordingly, they display variable reactivity with cellulose, affecting its performance after grafting. The influence of the structural characteristics of the grafted moieties (HA, SA, and VA) and chain segments of the cellulose were studied as far as changes in structure, elemental composition, and bonding after modification. After removal of any residual acids and ILs, the given systems were cast into all-cellulose films. Most notably, ILs and excess acids were easily recovered and recycled after gelling and regeneration of cellulose through a simple purification step. The properties of the three types of acids grafted on the cellulose films were compared with respect to morphology, crystallinity, transmittance, hydrophobicity, and processability. The IL-mediated modification with phenolic acids of cellulose allowed new types of films that favorably compete with petroleum-based plastics aimed for packaging.

EXPERIMENTAL SECTION

Materials. Unrefined, bleached softwood pulp board were kindly supplied by the Institute of Chemical Industry of Forestry Products, Chinese Academy of Forestry, and used as the cellulose precursor material. The pulp board was first cut into small segments and ground to obtain a loose powder before its dissolution. $[N_{4444}][OAc]$ was purchased from Sigma-Aldrich (Santa Clara). *p*-Hydroxybenzoic acid (HA), vanillic acid (VA), and syringic acid (SA) were purchased from Alfa Aesar (Karlsruhe, Germany). Acetone and dimethyl sulfoxide were obtained from Sinopharm Chemical Reagent Co. Ltd. (Shanghai, China). Other chemicals and solvents were of analytical reagent grade. All chemicals were used without further purification.

Homogeneous-Phase Modification of Cellulose. The $[N_{4444}][OAc]$/DMSO IL system was prepared according to our previously reported procedure.[22] In short, 10 mL of $[N_{4444}][OAc]$/DMSO (8:92 wt %) was used to obtain a 4 wt % cellulose solution upon stirring at room temperature for 30 min. Concurrently, in a separate flask, 0.2 g of either HA, VA, or SA, applied in solid form, was dissolved in 5 mL DMSO. The respective acid solution was added to the cellulose solution, thereby lowering its viscosity, which facilitated homogeneous reaction in an oil bath at 120 °C and under stirring at 600 rpm. The reaction was stopped after 3 h by centrifugation at 12 500 rpm with DMSO to remove undissolved and impurities.

Cellulose Films. The protocol used to homogeneously modify cellulose and prepare the respective films is shown in Figure 1. Fifteen

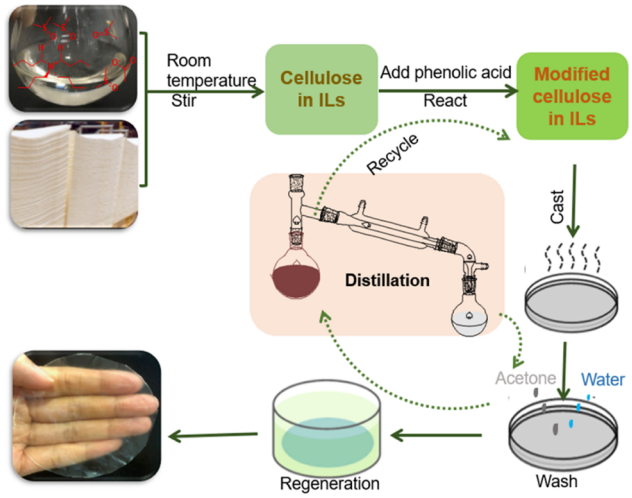

Figure 1. Preparation of the cellulose films modified with phenolic acid (HA, VA, or SA), using IL electrolyte as the solvent. Also shown is the process used to recycle the ILs, acids, and acetone.

milliliters of the respective solution was cast on Petri dishes (polystyrene; 100 mm diameter) and dried in an oven at 70 °C for 12 h, which allowed gelation (yielding gel suspensions), involving the partial dissolution and swelling of cellulose. Then, the films were formed by the regeneration of dissolved cellulose at room temperature followed by multiple washings with acetone (nonsolvent) to remove residual acid. The films were then immersed in a large amount of water, which was exchanged every day for 1 week until the respective hydrogel film achieved equilibrium. The gel films were then dried in ambient air for 72 h. In addition, films of neat cellulose were prepared as the reference using a similar procedure: A total of 4 wt % of same cellulose material was submerged in 10 mL of 8 wt % $[N_{4444}][OAc]$/DMSO solution and stirred at room temperature for 30 min. Concurrently, 5 mL DMSO was added to cellulose $[N_{4444}][OAc]$/DMSO solution; the mixture was then placed in an oil bath at 120 °C and stirred at 600 rpm for 3 h. After oven drying at 70 °C for 12 h, the

DOI: 10.1021/acs.biomac.9b00325
Biomacromolecules 2019, 20, 2105−2114

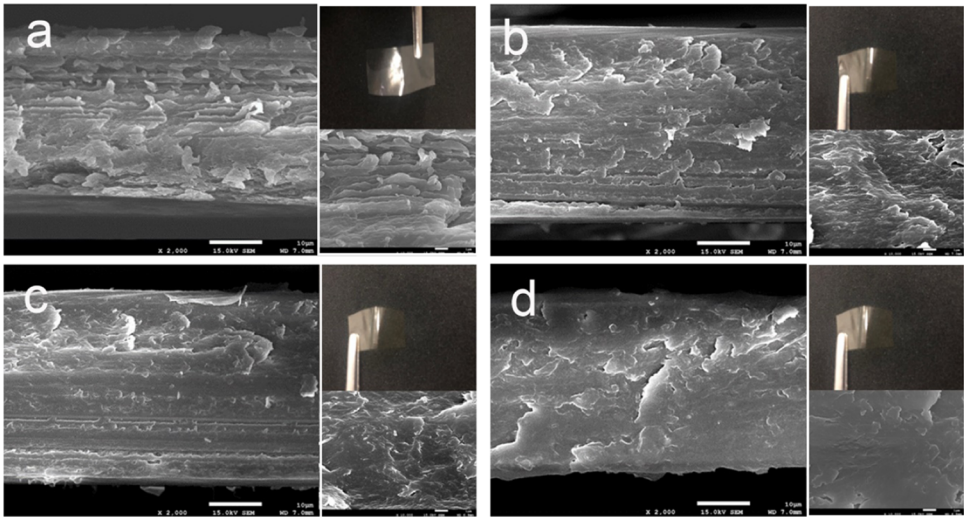

Figure 2. SEM cross-sectional structure at different magnifications (×2000) of CEL (a), H-CEL (b), V-CEL (c), and S-CEL (d) (photos of the films are shown on the right side of each image along with SEM images of higher magnification, ×10 000).

pure cellulose films were washed with acetone and water, dried again, and labeled as CEL. Accordingly, the respective dried films obtained after homogeneous modification of cellulose film samples are therein referred to as H-CEL, S-CEL, and V-CEL, corresponding to modification with HA, SA, and VA, respectively.

IL, Solvent, and Acid Recovery. The washing fluids, water, acetone, unreacted acids, $[N_{4444}][OAc]$, and DMSO were subjected to recovery. Acetone was first evaporated using the rotary evaporator, then the remaining effluent was oven-dried to remove water and residual DMSO. The solid phase comprised the respective acid and $[N_{4444}][OAc]$. The collected acids, $[N_{4444}][OAc]$, and acetone could be reused for several cycles to enable reprocessing (reaction and washing) as shown in Figure 1.

Morphological Analysis. The cross sections of the prepared films were observed under a JSM-7600F SEM (JEOL, Japan). The films were frozen and then fractured in liquid nitrogen. The cross sections of the fractured films were mounted on aluminum stubs with a carbon tape and coated with gold for 1 min (5−10 nm thickness) and then imaged with an accelerating voltage of 3−5 kV.

X-ray Photoelectron Spectroscopy and Elemental Analysis. Surface composition of pure CEL and modified cellulose (H-CEL, V-CEL, and S-CEL) were recorded with monochromatic A1 Kα irradiation at 100 W and effectively charged to neutralization with slow thermal electrons, using AXIS Ultra instrument (Kyoto, Japan). C−C/C−H assigned to the C 1s signal was set at 285.0 keV. XPS PEAK 41 program was used for the spectrum decomposition for C 1s, with the subtraction of a Shirley background before Gaussian functions. The degree of surface substitution (DS_S) was calculated from eq 1[23]

$$DS_S = C(O - C{=}O)/(C_{cellulose}/6) \quad (1)$$

where C(O−C═O) is the percentage of O−C═O groups from the grafted acids and $C_{cellulose}$ is the percentage of the C−O and O−C−O groups.

The DS in the bulk was also calculated from elemental analysis by using a Vario Macro cube elemental analyzer (Elementar, Fulda, German) which was used to determine the carbon, hydrogen, nitrogen, and oxygen content in the unmodified and modified celluloses (H-CEL, V-CEL, and S-CEL).

Nuclear Magnetic Resonance (NMR). Liquid-state NMR spectra were acquired on a Bruker AVANCE NEO 600 MHz spectrometer equipped with a 5 mm SmartProbe. The samples were dissolved in the ionic liquid electrolyte, tetrabutylphosphonium acetate ($[P_{4444}][OAc]$):DMSO-d_6 (20:80 wt %), according to a published procedure.[24] However, the final 5 wt % viscosity was too high due to the high molecular weight of the materials, preventing transfer to the 5 mm NMR tube and likely offering poor resolution. This is typical of Kraft pulps. Therefore, the sample was diluted with further $[P_{4444}][OAc]$:DMSO-d_6 electrolyte to a concentration of ∼3 wt %. ^{1}H and diffusion-edited[23] ^{1}H experiments were collected for CEL, H-CEL, V-CEL, and S-CEL. The diffusion-edited ^{1}H was used to filter out the low-molecular-weight species in the sample to allow for identification of the polymeric species that may not be visible under the H_2O or $[P_{4444}][OAc]$ signals. A multiplicity-edited heteronuclear single quantum coherence (HSQC) for S-CEL was collected to help identify the cellulosic resonances and those of other potential impurities. Full details of the NMR experimental conditions and pulse sequences are given in the Supporting Information, which also includes measurements via ^{13}C CP (cross-polarization) MAS (magic-angle spinning) NMR.

Water Contact Angle (WCA). The water contact angle (WCA) was determined using an optical contact angle meter SL 100 B from Solon Information Technology Co., Ltd. (Shanghai, China) at a RH of 50% and 23 °C. To compare different samples, each contact angle was taken at 60 s, and the average value of at least three measurements is presented.

Barrier Properties. Water vapor sorption (WVP) of the films was measured by a Bei Shide 3H-2000 PW dynamic vapor sorption analyzer. The temperature and the relative humidity (RH) were set at 25 °C and 50%, respectively, to obtain the equilibrium adsorption capacity. At least three samples were characterized.

Water Absorption. Film water absorption was determined by placing circular film (4 cm diameter) into 10 cm diameter Petri dishes containing 30 mL deionized water. The weight of the film before and after 30 min immersion was obtained to determine the amount of water absorbed. The water absorption rate was calculated based on the change in weight with time.

Mechanical Properties. The mechanical properties, including the tensile stress, tensile strain, and Young's modulus of the films were measured using a mechanical testing unit (Shenzhen, China). Specimens, 40 × 10 mm^2, were cut at random positions on the films and conditioned for 1 day at 23 °C and 50% RH. A gauge length of 10 mm, a 500 N loading cell, and a cross-head speed of 5 mm/min were used. The thickness of the specimens was measured at five random locations for each film (NSK micrometer, Japan). At least 10 samples of each film were tested, and the average values are reported with the standard deviation.

X-ray Diffraction. X-ray diffraction (XRD) patterns were obtained at room temperature using an Ultima IV X-ray diffractometer (RigaKu, Tokyo, Japan) with Cu Kα at a 40 kV acceleration voltage and a 30 mA current. The diffraction was recorded at a scan rate of 5° min^{-1} in the range of 2Θ = 5−30°.

DOI: 10.1021/acs.biomac.9b00325
Biomacromolecules 2019, 20, 2105−2114

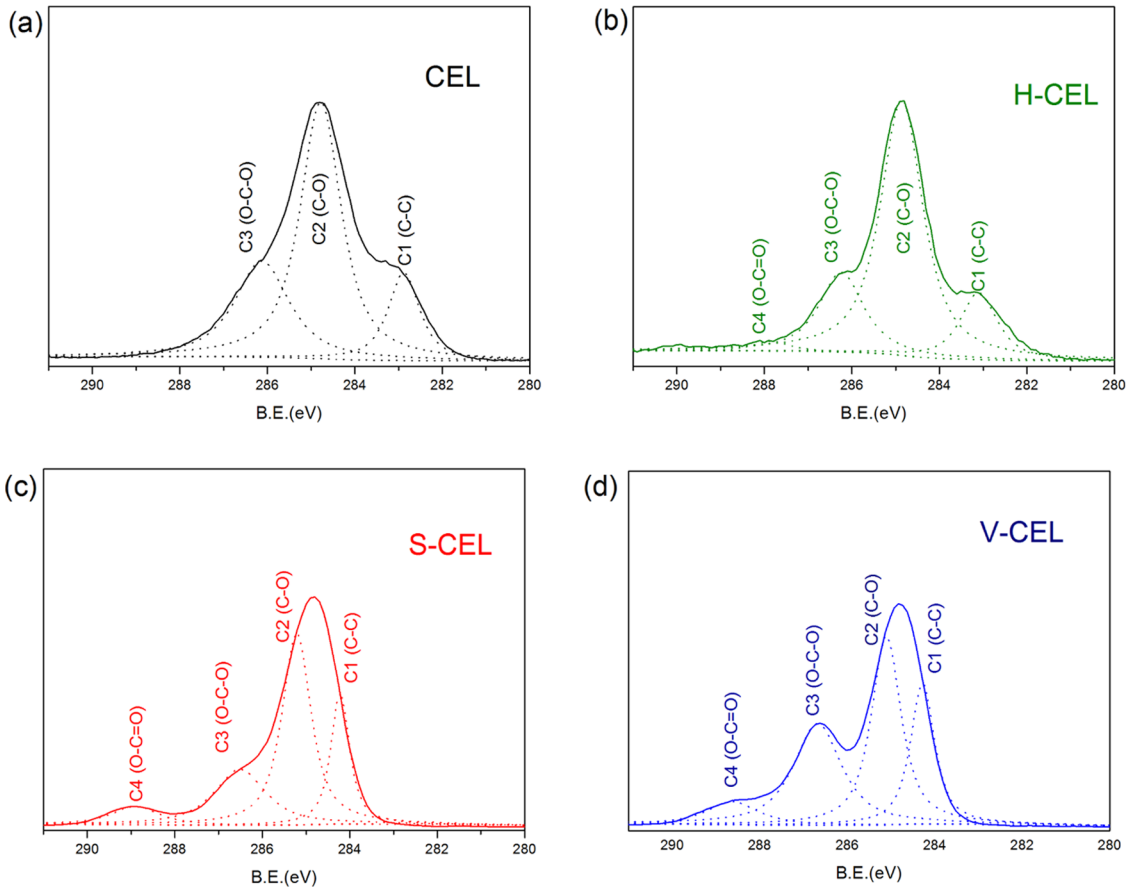

Figure 3. Deconvolution of C 1s spectra of (a) CEL, (b) H-CEL, (c) S-CEL, and (d) V-CEL films.

Transmittance. The transparency of the films was measured using a UV−vis spectrophotometer (Shimadzu UV-240, Japan). The transmittance spectra of the samples over the 400−800 nm range was recorded. Film specimens were cut into rectangular shapes and placed in an integrating sphere; three duplicates of each sample were analyzed and transmittance was normalized by the respective thickness of the film to account for the small differences in this parameter.

RESULTS AND DISCUSSION

Morphology of CEL and Modified Cellulose Films. Typical CEL films show a layered structure formed by randomly oriented fibrils, as revealed by cross-sectional images (SEM; Figure 2a). Clear features are observed with sizes in the micro- and nanometer scales. Compared to the film of unmodified cellulose, CEL (35 μm), the samples treated with acids (Figure 2b−d) were denser according to the following order: H-CEL (33 μm) < V-CEL (31 μm) < S-CEL (29 μm). The results indicate a high degree of uniformity. Layering is observed for H-CEL, V-CEL, but this is less evident in the case of S-CEL (Figure 2d). The observed morphologies are a result of the partial disintegration of the crystalline and amorphous domains of cellulose caused by esterification and oxidation reactions,[25] as well as the partial homogeneous dissolution of cellulose in ionic liquids, ILs, which "welded" the rest of the components.

Extent of Chemical Grafting. As shown in Figure 1, the IL-mediated modification of cellulose films took place by reaction between partly dissolved cellulose and the acids that were dissolved in $[N_{4444}][OAc]$/DMSO solution, followed by evaporation of the solvent at a relatively high temperature, and swelling of the cast film in water until an equilibrium state was achieved. The successful esterification of cellulose is confirmed by comparing the FTIR spectra of CEL and the modified cellulose samples (H-CEL, S-CEL, and V-CEL; Figure S1). In FTIR, peaks appearing at 1700−1800 cm^{-1} are characteristic of C═O stretching in esters, acids, and other carbonyls.[26] By comparing the modified samples with CEL, an additional shoulder on the main C═O stretching peak is noted at 1720 cm^{-1}, clearly indicating a low degree of esterification. In addition, the peak range of 1200−1500 cm^{-1} is characteristic for different cellulose crystalline allomorphs.[27] This shows changes between the modified and unmodified CEL samples.

Further confirmation of esterification is given via high-resolution carbon C 1s XPS spectroscopy, which is a surface technique with a penetration depth of few nanometers. The deconvolution of C 1s spectra for CEL, H-CEL, V-CEL, and S-CEL are included in Figure 3. The neat CEL has three distinctive peaks with binding energies (BE) corresponding to 284.4 (C−C, C−H), 285.6 (C−O), and 287.6 (C−O−C) eV, which are consistent with the reported data.[28,29] The C 1s spectra of modified CELs have an additional peak at 288.7 eV, corresponding to three neighboring oxygens that confirm the esterification. The differences in the C−O═O peaks in Figure 3b−d indicate the different extents of esterification at the film surfaces. In modified CELs, the area and intensities of some peaks increased, whereas a slight shift in their position took place. The C1 and C2 peaks of untreated cellulose shifted toward higher BE, which can be attributed to a change in its environment after modification. The clearly visible increase in the C4 (O−C═O) peak area, most obvious for V-CEL and S-

DOI: 10.1021/acs.biomac.9b00325
Biomacromolecules 2019, 20, 2105−2114

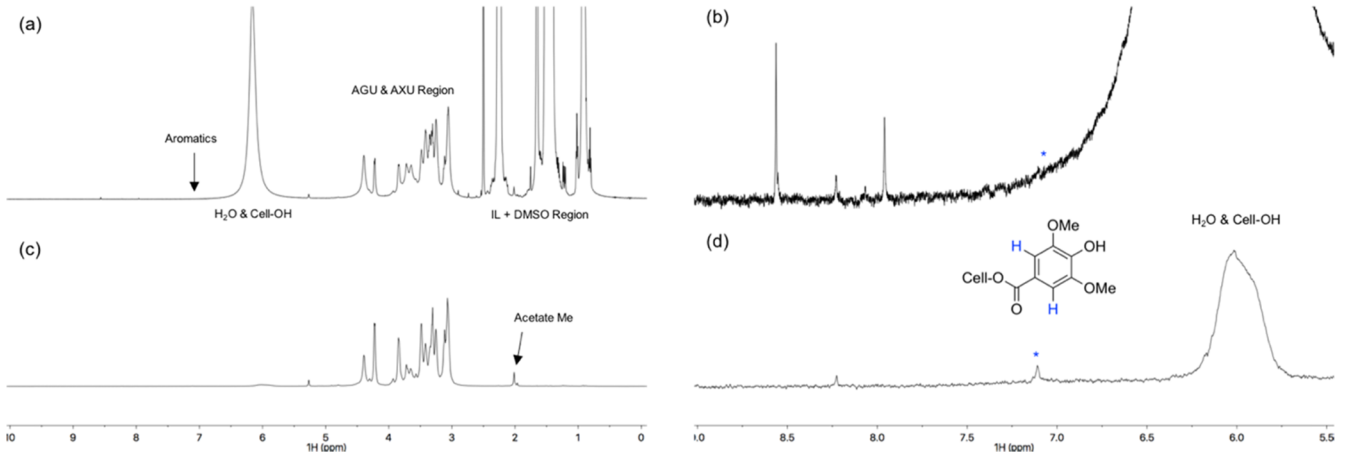

Figure 4. ^{1}H and diffusion-edited ^{1}H NMR spectra of bulk S-CEL film, dissolved in the $[P_{4444}][OAc]$:DMSO-d_6 electrolyte at 65 °C: (a) full spectral region for the standard ^{1}H experiment, (b) expanded aromatic region for the standard ^{1}H experiment, (c) full spectral region for the diffusion-edited ^{1}H experiment, and (d) expanded aromatic region for the diffusion-edited ^{1}H experiment. AGU and AXU refer to anhydroglucose and anhydroxylose units, respectively.

CEL, clearly suggests the occurrence of esterification. Based on the deconvolution of the C 1s peak, the C4 percentage on the surface of H-CEL, V-CEL, and S-CEL is 6.4, 7.3, and 7.8%, respectively. The relative intensity of the C4 peaks on the surface of the samples directly relate to the degree of substitution (DS) on the CEL; thus, it is reasonable to assume that S-CEL possesses the highest DS.

For elemental analysis of CEL, H-CEL, V-CEL, and S-CEL, the films were dried to constant weight before testing. Theoretically, the surface C/O ratio for the HA, VA, and SA moieties grafted on cellulose should gradually rise. However, the experimental C/O ratio values for H-CEL, V-CEL, and S-CEL films (Table S1) were not significantly different (0.85), probably owing to the low bulk DS values (DS < 0.25, Table S1). Elemental analysis also shows the presence of nitrogen, which may originate from traces of IL left in the sample.

To further confirm the esterification of the films, a novel liquid-state NMR method was used by direct dissolution of the films into the IL electrolyte $[P_{4444}][OAc]$:DMSO-d_6.[24] Comparison of the standard ^{1}H and diffusion-edited ^{1}H spectra for all CEL samples was performed to identify the polymeric ester species in the samples. The diffusion-edited experiments almost completely eliminate the low-molecular-weight species (i.e., H_2O, IL, and DMSO) from the spectra, leaving only the polymeric resonances behind. The ^{1}H NMR spectra for S-CEL are shown in Figure 4, with the spectra for the remainder of the CEL samples in the Supporting Information (Figure S2). The CEL ^{1}H spectra show overlapping peaks characteristic of the anhydroglucose (AGU) and anhydroxylose (AXU) units from the fibers (3−4.5 ppm).[30] The $[P_{4444}][OAc]$:DMSO-d_6 resonances appear from 0.8 to 2.5 ppm, overlapping with the acetate region (2.0 ppm), and the aromatic resonances are expected to be between 6.5 and 8 ppm, somewhat overlapping with the H_2O peak. The diffusion-edited spectra (Figure 4c) clearly show the presence of polymeric acetate (2.0 ppm). Integration of the C1 region (4.25−4.75 ppm) vs the acetate region in the standard ^{1}H spectrum results in a very rough molar ratio of acetate to C1 of 0.01 (1%). The diffusion-edited spectrum gives a value of ∼0.03 but is known to overestimate species that have slower T_2 relaxation rates, such as rapidly rotating methyl groups. By analyzing the expanded aromatic region (Figure 4d), there is a peak at 7.11 ppm, which is consistent with a literature assignment (methyl syringate, 7.32 ppm, $CDCl_3$)[31] for the aromatic C−H of the syringyl ester attached to the polymer. However, the intensity of the peak is rather low, indicating up to ∼0.005 (0.5%) molar equivalents vs C1. H-CEL and V-CEL (Figures S3 and S4) show similar assignments for the presence of acetate and phenolic esters. V-CEL and S-CEL show the highest degrees of esterification, mainly with acetate. By contrast, CEL, which was not contacted with phenolic acids, does not show any esterification, even with acetate. Thus, esterification is shown to have occurred, but it was preferential for the acetate, derived from the $[N_{4444}][OAc]$ IL. Such low degrees of esterification are not unexpected, as electrolytes capable of dissolving cellulose are typically quite basic, whereas Fischer esterification is only greatly enhanced with acid catalysts. With the presence of the phenolic acids, there is clearly some degree of autocatalysis, which may be leveraged in the future to increase the DS values and film properties.

A more thorough characterization of the cellulosic spectral regions (^{1}H and ^{13}C) was performed by collecting a multiplicity edited HSQC spectrum of S-CEL at 75 °C in the electrolyte (Figure 5). Seventy-five degree Celcius was used to slightly improve the signal-to-noise ratio and resolution. This allowed for the identification of the major anhydroglucose unit (AGU) and anhydroxylose unit (AXU) resonances, which are consistent with previous assignments.[30] Additional prominent resonances are apparent. A geminal peak at 3.35/62.84 ppm seems to be consistent with the α-CH_2 of the $[N_{4444}]$ cation. An additional peak at 3.32/57.39 ppm is the likely residual solvent and might be consistent with traces of contaminating ethanol. Due to the low abundance of ester apparent from the liquid-state NMR, S-CEL was also analyzed by ^{13}C CP-MAS (Figure S5) to confirm the liquid-state NMR results. This also confirms a very low ester carbonyl peak (174 ppm), indicating a low degree of esterification. Aliphatic carbon peaks at 12.5−30 ppm also seem to correspond nicely with carbonyl Me and $[N_{4444}]$ cation, confirming the presence of residual IL cation, which was not washed away completely during the film preparation. In addition, there seems to be a very low level of cellulose I crystallinity from the C4 peak shape (85−92 ppm), which seems to be more akin to a low degree of cellulose II crystallinity.[32]

DOI: 10.1021/acs.biomac.9b00325
Biomacromolecules 2019, 20, 2105−2114

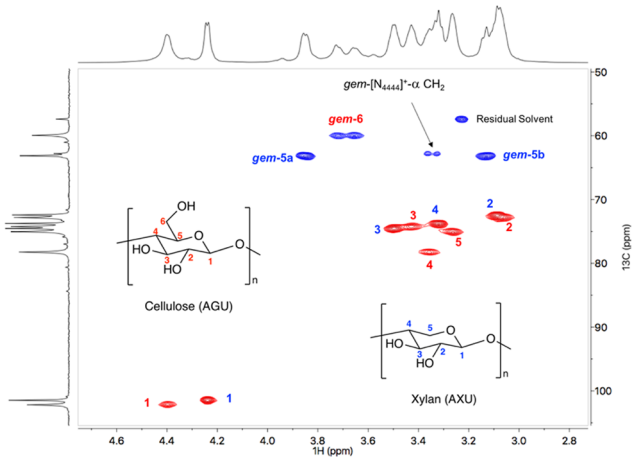

Figure 5. Multiplicity-edited $^{1}H-^{13}C$ HSQC NMR spectrum for the bulk S-CEL film, dissolved in the $[P_{4444}][OAc]$:DMSO-d_6 electrolyte at 75 °C. Red is CH/CH_3 and blue is CH_2. "*gem*" refers to geminal. The ^{1}H trace is the diffusion-edited experiment. AGU refers to the anhydroglucose unit. AXU refers to the anhydroxylose unit.

Overall, the NMR results clearly indicate low degrees of reaction, as would be expected under these conditions but also reflected the changes in crystallinity upon the dispersion and gelation stages. Figures 3, 4, 5, S1, S2, S3, S4, S5, and Table S1 confirm that all phenolic acids were grafted on CEL with well-defined structures. The degree of esterification for each film is relatively low and can be listed in the order CEL < H-CEL < V-CEL < S-CEL. Such an observation is ascribed to the different electrostatic and steric effects brought about each of the phenolic acids used for modification, according to the reactivity of the respective carboxylic groups.[33−35]

Film Hydrophobicity and Barrier Properties. The water contact angle (WCA) of the CEL film was measured 1 min after droplet deposition. A WCA of 42° was comparable to other cellulosic materials and, in particular, films obtained after the dissolution of cellulose in the *N*-methyl morpholine-*N*-oxide/DMSO system.[36] Upon acid grafting, the WCA increased; such a reduction of hydrophilicity correlates with the DS_S results (Figure 6): the highest WCA (86°) was measured for S-CEL (DS_S, 0.68), which contained more aromatic rings attached to the surface. The DS and DS_S values confirm that the grafting makes the cellulose film more

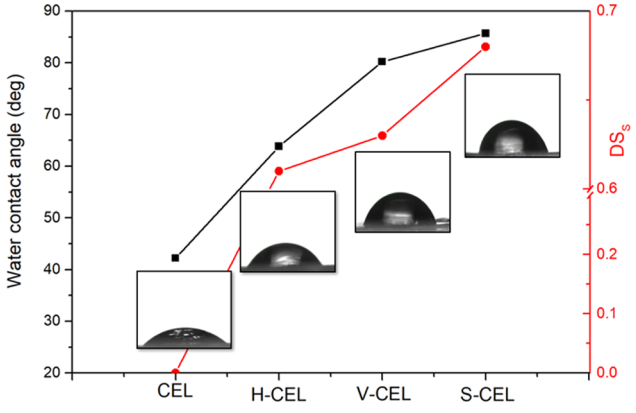

Figure 6. Water contact angle (images shown in the inset) and degree of surface substitution (DS_s) obtained by XPS for CEL, H-CEL, V-CEL, and S-CEL films.

hydrophobic in the order S-CEL > H-CEL > V-CEL. Noticeably, the values of DSs calculated by XPS were significantly higher compared to the DS obtained by elemental analysis (bulk DS < 0.25; Table S1). This can be taken as an evidence of the enrichment of esters at the surface of the films.

The neat CEL film absorbed more water than that after IL-mediated modification. The equilibrium water adsorption after 30 min was reduced significantly, from the original 86 to 50−70%. The water uptake of the original fibers correlated with the contribution of amorphous structures and porosity, which facilitate water penetration into the film. Regenerated cellulose generally has lower crystallinity and absorbs more moisture than wood fibers. From the SEM results, acid-grafted CEL films were significantly denser compared to the CEL sample. The reaction in ILs resulted in welding; therefore, a lower porosity was observed in the films, which would reduce the water absorption. Moreover, the S-CEL sample, which presented a large number of $-OCH_3$ groups on the cellulose, led to the most hydrophobic films.

Due to the hydrophilic nature of cellulose, pure cellulose films have poor water-vapor-barrier properties. However, in practical applications, high water-vapor-barrier properties are required for materials used in electronic and packaging materials. After IL treatment, CEL and acid-grafted CEL films had a water transmittance rates in the range of 1000−3000 g·μm/m^2·day·kPa, lower than that of other films prepared with cellulose nanomaterials (Table 1).[37] The values of WVP

Table 1. Density, Porosity, Water Absorption, and Water Vapor Permeability of CEL, H-CEL, V-CEL, and S-CEL Films

film	density (g·cm^{-3})	porosity (%)	water absorption (%)	WVP (g·μm/m^2·day·kPa)
CEL	0.92	31.3	84.1	2881
H-CEL	0.95	29.1	66.2	1689
V-CEL	1.02	23.8	56.6	1240
S-CEL	1.09	15.8	50.8	1069

decreased in the order H-CEL > V-CEL > S-CEL. In the case of the S-CEL films (1069 g·μm/m^2·day·kPa), a high water barrier at 50% RH was also observed. The water vapor permeability measured at 23 °C and 50% RH of the acid-grafted cellulose films was slightly higher than those of commercial polymer films (for example, poly(lactic acid) (PLA): 898 g·μm/m^2·day·kPa[38] and polyhydroxyalkanoate, PHA: 824 g·μm/m^2·day·kPa[39]). However, the barrier performance of V-CEL and S-CEL films was slightly better than that measured for composite films of PLA reinforced with 15% cellulose nanocrystals (CNC) (1901 g·μm/m^2·day·kPa),[40] as well as polycaprolactone (PCL) reinforced with 5% CNC (1510 g·μm/m^2·day·kPa).[41]

Mechanical Properties. Typical tensile profiles and the average value of elongation at break and Young's modulus are presented in Figure 7. For CEL films, the tensile strength, modulus, and strain at failure were 99 MPa, 3.4 GPa, and 3.4%, respectively, which are characteristic of a fragile material. In contrast, the modification of CEL improved the toughness, with a significant improvement in ductility for H-CEL, V-CEL, and S-CEL (an increased strain of 571, 760, and 808%, respectively). Moreover, the acid treatment of CEL resulted in only a slight decrease in strength, from 100 to 80−90 MPa. The increased strength accompanied by a simultaneous

DOI: 10.1021/acs.biomac.9b00325
Biomacromolecules 2019, 20, 2105−2114

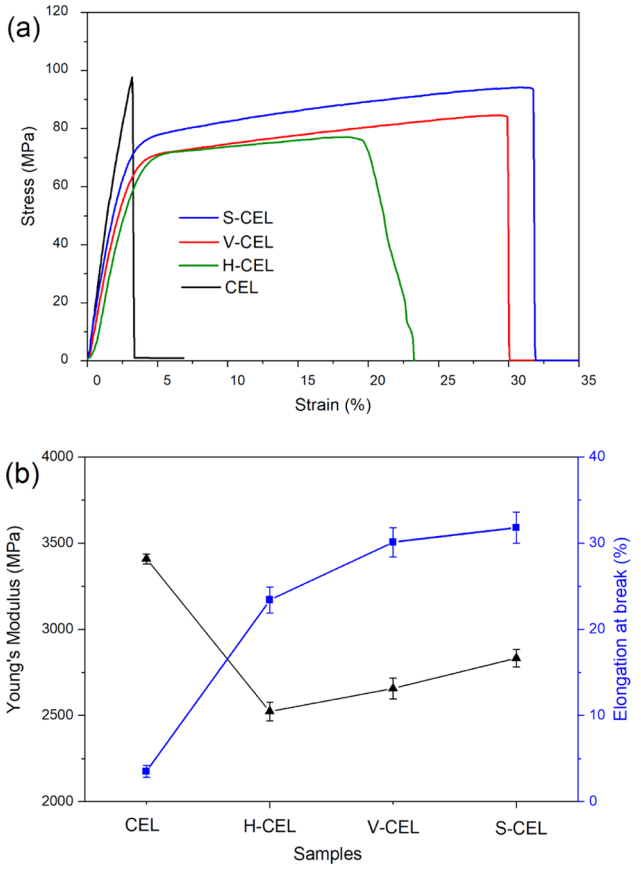

Figure 7. Tensile strength of CEL, H-CEL, V-CEL, and S-CEL films: tensile stress−strain curves (a) and measured Young's modulus and elongation at break (b). Error bars correspond to the calculated standard deviation.

improvement in toughness is ranked according to S-CEL> H-CEL > V-CEL. The relatively high strength of V-CEL and S-CEL films is explained by the high density of grafted, rigid phenolic structures (1,2-OCH_3 on the benzene ring) and the −OH from phenolic acids that contribute to hydrogen bonding with cellulose. Most distinctive, the trend implies an increased stiffness with a simultaneously more stretchable film, which is rarely reported for nanofiller-reinforced composites.

After modification in ILs, the modified CEL films displayed a slight decrease in Young's modulus compared to that of CEL, which is probably associated with the change in the crystalline structure caused by the dissolving−regeneration process and the effect of excess acids. Possible explanations for this observation are that the ILs, known as efficient solvents of cellulose, could swell the compact structure of cellulose fiber and may have converted microsized fibers or fiber clusters into nanosized fibrils, which resulted in the reduction in crystallinity or conversion to cellulose II, and simultaneously increased surface area for stress transfer.[42] Additionally, the IL could work as a welding agent,[43] creating disordered cellulose domains on the surface of the nanosized fibrils, connecting them together, and forming a continuous and integrated network. During the welding process, the bulk and surface of the cellulose was likely plasticized by ILs and became more flexible. Moreover, as can be seen in Table 1, the density of the films increased from the original 0.92 to 0.95, 1.02, and 1.09 g·cm^{-3} for CEL, H-CEL, V-CEL, and S-CEL, respectively. The film with the highest density was S-CEL, possibly indicative of increased reactivity in the presence of syringic acid.

Film Crystallinity. Wide-angle X-ray diffraction patterns of the raw fibers and modified CEL films clearly show changes in crystallinity (Figure 8). The CEL film shows the presence of

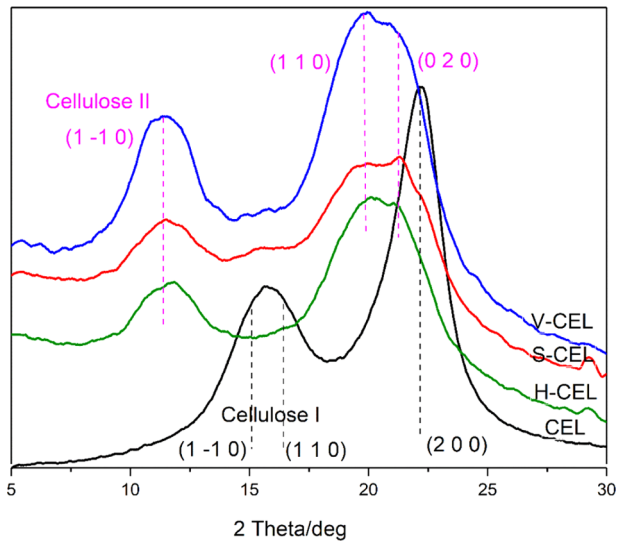

Figure 8. Wide-angle X-ray diffraction spectrogram of CEL, H-CEL, V-CEL, and S-CEL films.

native cellulose I crystalline allomorph. In contrast, H-CEL, V-CEL, and S-CEL films showed a clear reduction in crystallinity and recrystallization to the cellulose II crystalline allomorph.[44]

Small diffraction peaks of (110) and (200) from the native cellulose I allomorph were detected in the XRD patterns of the acid-modified cellulose films. It is noteworthy that the V-CEL showed the largest degree of cellulose II crystallinity, then the S-CEL, and H-CEL. These results indicate increased crystalline components in the films with increasing aspect ratios of the crystal of cellulose II,[45] which explains the observed improvement in the stiffness of the acid-modified cellulose films.

Light Transmittance. UV−vis spectroscopy confirmed a high light transmittance for all films over the entire range of visible and near-infrared light (Figure 9). Neat CEL films prepared in [N_{4444}][OAc]/DMSO system (average thickness

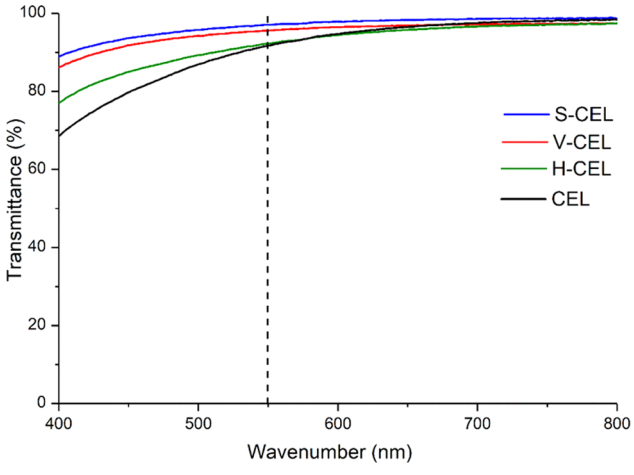

Figure 9. Light transmittance (at visible range) results of CEL, H-CEL, V-CEL, and S-CEL films.

DOI: 10.1021/acs.biomac.9b00325
Biomacromolecules 2019, 20, 2105−2114

of 30 μm), for example, had a light transmittance of 88% at 550 nm, which is higher than most of the other all-cellulose composite films containing native or regenerated cellulose fibers. The transparency of all-cellulose films have been reported to be ~80% (170 μm thickness),[46] >80% (140 μm thick films of NaOH-treated cellulose fibers),[47] up to 88% (30 μm thick TEMPO-oxidized cellulose nanofiber films),[48] and 85% for films obtained from regenerated cellulose.[49] The higher transparency of the modified cellulose films indicates a highly uniform structure. The porosity (reduced porosity of the modified cellulose films), from 31% in CEL to 15% in S-CEL, correlate with a reduced light scattering at the fibril interfaces and the contribution of voids.[50]

Chemical Recovery. Chemical recovery is important under the concept of green chemistry. Based on our previous work, $[N_{4444}][OAc]$/DMSO is an effective solvent for dissolving cellulose, and it is relatively stable during processing.[22] Therefore, the reusability of $[N_{4444}][OAc]$ and the acids was assessed upon washing with modified CEL films with an organic solvent (acetone). The recovery procedure, shown in Figure 1, included acetone direct distillation (rotary evaporation), whereas the crude acids and $[N_{4444}][OAc]$ were recovered by oven-drying the residuals. The solid phase comprised the respective acid and $[N_{4444}][OAc]$, which were extracted with dichloromethane after washing several times with distilled water for further purification. It was found that the recovery rate of $[N_{4444}][OAc]$ was >90% (for a purity of ~40%). The synthesis of new films was demonstrated by recycling the recovered chemicals, indicating the promise of $[N_{4444}][OAc]$ and the used phenolic acids for such purpose. Naturally, the efficiency of the system diminished with the number of cycles.

CONCLUSIONS

Inspired by the composition and structure of plant's cell wall, cellulosic fibers were modified with phenolic acids in low-concentration IL electrolyte systems under homogeneous conditions. Extended gelation and regeneration resulted in less hydrophobic films. Despite the low degree of esterification, the films displayed remarkable mechanical performance and optical transparency. No additional catalyst was used to enable the Fischer esterification reaction, indicating the reaction was autocatalytic. This is beneficial for the recyclability of the system, as components are kept to a minimum, which requires only some solvent evaporation and acid makeup. The products were characterized by FT-IR, XPS, elemental analyses, liquid-state NMR, and solid-state NMR to understand the reactivity. Highly transparent films (H-CEL, V-CEL, and S-CEL) with a thickness of 30 μm were obtained easily by casting. The acid-modified cellulose films possessed excellent mechanical strength, with a Young's modulus of 2−3.5 GPa and a strain at break of up to 35%. The films were flexible and tough, superior to those of paper and most other reported all-cellulose films. The excellent mechanical properties achieved owes to the synergistic effect of esterification, morphology, and porosity changes (electrolyte "welding" effect). NMR vs XPS suggests a possible enrichment of ester at the film surface. In addition, the films showed good hydrophobicity and barrier properties, which are highly favorable for application in biobased plastics, packaging materials, optical and electronic devices.

ASSOCIATED CONTENT

Supporting Information

The Supporting Information is available free of charge on the ACS Publications website at DOI: 10.1021/acs.biomac.9b00325.

Description of FT-IR and elemental analysis methods; table of elemental content in films; FT-IR spectra; ^{1}H NMR spectra of bulk CEL, H-CEL, and V-CEL films, and ^{13}C CPMAS NMR spectra of S-CEL films (PDF)

AUTHOR INFORMATION

Corresponding Authors

*E-mails: hpan@njfu.edu.cn (H.P.).
*E-mails: orlando.rojas@aalto.fi (O.J.R.).

ORCID

Alistair W. T. King: 0000-0003-3142-9259
Sami Hietala: 0000-0003-1448-1813
Hui Pan: 0000-0001-5074-8314
Orlando J. Rojas: 0000-0003-4036-4020

Notes

The authors declare no competing financial interest.

ACKNOWLEDGMENTS

H.P., X.N., and Y.L. are grateful for the financial support by the Forestry Industry Research Special Funds for Public Welfare Projects (201504602), Nature Science Foundation of China (31770631), and the Priority Academic Program Development (PAPD) project of Jiangsu Higher Education Institutions. O.J.R. and X.N. acknowledge funding support by European Research Council (ERC) under the European Union's Horizon 2020 research and innovation program (ERC Advanced Grant agreement No. 788489, "BioElCell"). A.W.T.K. acknowledges funding support from the Finnish Academy under the project "WTF-Click-Nano" (311255).

REFERENCES

(1) Torres-Rendon, J. G.; Femmer, T.; De Laporte, L.; Tigges, T.; Rahimi, K.; Gremse, F.; Zafarnia, S.; Lederle, W.; Ifuku, S.; Wessling, M.; Hardy, J. G.; Walther, A. Bioactive gyroid scaffolds formed by sacrificial templating of nanocellulose and nanochitin hydrogels as instructive platforms for biomimetic tissue engineering. *Adv. Mater.* **2015**, *27*, 2989−2995.

(2) Lin, Y.; Gritsenko, D.; Liu, Q.; Lu, X.; Xu, J. Recent Advancements in Functionalized Paper-Based Electronics. *ACS Appl. Mater. Interfaces* **2016**, *8*, 20501−20515.

(3) Wang, S.; Li, T.; Chen, C.; Kong, W.; Zhu, S.; Dai, J.; Diaz, A. J.; Hitz, E.; Solares, S. D.; Li, T.; Hu, L. Transparent, Anisotropic Biofilm with Aligned Bacterial Cellulose Nanofibers. *Adv. Funct. Mater.* **2018**, *28*, No. 1707491.

(4) Toivonen, M. S.; Kaskela, A.; Rojas, O. J.; Kauppinen, E. I.; Ikkala, O. Ambient-Dried Cellulose Nanofibril Aerogel Membranes with High Tensile Strength and Their Use for Aerosol Collection and Templates for Transparent, Flexible Devices. *Adv. Funct. Mater.* **2015**, *25*, 6618−6626.

(5) Li, Y.; Xiao, H.; Pan, Y.; Wang, L. Novel Composite Adsorbent Consisting of Dissolved Cellulose Fiber/Microfibrillated Cellulose for Dye Removal from Aqueous Solution. *ACS Sustainable Chem. Eng.* **2018**, *6*, 6994−7002.

(6) Baidya, A.; Ganayee, M. A.; Ravindran, S. J.; Tam, K. C.; Das, S. K.; Ras, R. H. A.; Pradeep, T. Organic Solvent-Free Fabrication of Durable and Multifunctional Superhydrophobic Paper from Water-borne Fluorinated Cellulose Nanofiber Building Blocks. *Acs Nano* **2017**, *11*, 11091−11099.

DOI: 10.1021/acs.biomac.9b00325
Biomacromolecules 2019, 20, 2105−2114

(7) Hakalahti, M.; Mautner, A.; Johansson, L. S.; Hanninen, T.; Setala, H.; Kontturi, E.; Bismarck, A.; Tammelin, T. Direct Interfacial Modification of Nanocellulose Films for Thermoresponsive Membrane Templates. *ACS Appl. Mater. Interfaces* **2016**, *8*, 2923−2927.
(8) Ye, C.; Malak, S. T.; Hu, K.; Wu, W.; Tsukruk, V. V. Cellulose Nanocrystal Microcapsules as Tunable Cages for Nano- and Microparticles. *Acs Nano* **2015**, *9*, 10887−10895.
(9) Farrán, A.; Cai, C.; Sandoval, M.; Xu, Y.; Liu, J.; Hernaiz, M. J.; Linhardt, R. J. Green solvents in carbohydrate chemistry: from raw materials to fine chemicals. *Chem. Rev.* **2015**, *115*, 6811−53.
(10) Mahmood, H.; Moniruzzaman, M.; Yusup, S.; Welton, T. Ionic liquids assisted processing of renewable resources for the fabrication of biodegradable composite materials. *Green Chem.* **2017**, *19*, 2051−2075.
(11) King, A. W. T.; Parviainen, A.; Karhunen, P.; Matikainen, J.; Hauru, L. K. J.; Sixta, H.; et al. Relative and inherent reactivities of imidazolium-based ionic liquids: the implications for lignocellulose processing applications. *RSC Adv.* **2012**, *2*, 8020−8026.
(12) Zhu, C.; Koutsomitopoulou, A. F.; Eichhorn, S. J.; van Duijneveldt, J. S.; Richardson, R. M.; Nigmatullin, R.; Potter, K. D. High Stiffness Cellulose Fibers from Low Molecular Weight Microcrystalline Cellulose Solutions Using DMSO as Co-Solvent with Ionic Liquid. *Macromol. Mater. Eng.* **2018**, *303*, No. 1800029.
(13) Abdel-Aal, E. A. M.; Choo, T. I.; Dhillon, S.; Rabalski, I. Free and Bound Phenolic Acids and Total Phenolics in Black, Blue, and Yellow Barley and Their Contribution to Free Radical Scavenging Capacity. *Cereal Chem. J.* **2012**, *89*, 198−204.
(14) Iiyama, K.; Lam, T. B. T.; Stone, B. A. Phenolic acid bridges between polysaccharides and lignin in wheat internodes. *Phytochemistry* **1990**, *29*, 733−737.
(15) Heleno, S. A.; Martins, A.; Queiroz, M. J.; Ferreira, I. C. Bioactivity of phenolic acids: metabolites versus parent compounds: a review. *Food Chem.* **2015**, *173*, 501−513.
(16) Rao, Y.; Zhao, X.; Li, Z.; Huang, J. Phenolic acids induced growth of 3D ordered gold nanoshell composite array as sensitive SERS nanosensor for antioxidant capacity assay. *Talanta* **2018**, *190*, 174−181.
(17) Rasheeda, K.; Bharathy, H.; Nishad Fathima, N. Vanillic acid and syringic acid: Exceptionally robust aromatic moieties for inhibiting in vitro self-assembly of type I collagen. *Int. J. Biol. Macromol.* **2018**, *113*, 952−960.
(18) Chatterjee, N. S.; Panda, S. K.; Navitha, M.; Asha, K. K.; Anandan, R.; Mathew, S. Vanillic acid and coumaric acid grafted chitosan derivatives: improved grafting ratio and potential application in functional food. *J. Food Sci. Technol.* **2015**, *52*, 7153−7162.
(19) Vishnu, K. V.; Chatterjee, N. S.; Ajeeshkumar, K. K.; Lekshmi, R. G. K.; Tejpal, C. S.; Mathew, S.; Ravishankar, C. N. Microencapsulation of sardine oil: Application of vanillic acid grafted chitosan as a bio-functional wall material. *Carbohydr. Polym.* **2017**, *174*, 540−548.
(20) Vishnu, K. V.; Ajeesh Kumar, K. K.; Chatterjee, N. S.; Lekshmi, R. G. K.; Sreerekha, P. R.; Mathew, S.; Ravishankar, C. N. Sardine oil loaded vanillic acid grafted chitosan microparticles, a new functional food ingredient: attenuates myocardial oxidative stress and apoptosis in cardiomyoblast cell lines (H9c2). *Cell Stress Chaperones* **2018**, *23*, 213−222.
(21) Benítez, A. J.; Walther, A. Cellulose nanofibril nanopapers and bioinspired nanocomposites: a review to understand the mechanical property space. *J. Mater. Chem. A* **2017**, *5*, 16003−16024.
(22) Huang, Y.-B.; Xin, P.-P.; Li, J.-X.; Shao, Y.-Y.; Huang, C.-B.; Pan, H. Room-Temperature Dissolution and Mechanistic Investigation of Cellulose in a Tetra-Butylammonium Acetate/Dimethyl Sulfoxide System. *ACS Sustainable Chem. Eng.* **2016**, *4*, 2286−2294.
(23) Bendahou, A.; Hajlane, A.; Dufresne, A.; Boufi, S.; Kaddami, H. Esterification and amidation for grafting long aliphatic chains on to cellulose nanocrystals: a comparative study. *Res. Chem. Intermed.* **2014**, 1−18.
(24) King, A. W. T.; Mäkelä, V.; Kedzior, S. A.; Laaksonen, T.; Partl, G. J.; Heikkinen, S.; et al. Liquid-state nmr analysis of nanocelluloses. *Biomacromolecules* **2018**, *19*, 2708−2720.
(25) Cheng, Q.; Ye, D.; Yang, W.; Zhang, S.; Chen, H.; Chang, C.; Zhang, L. Construction of Transparent Cellulose-Based Nanocomposite Papers and Potential Application in Flexible Solar Cells. *ACS Sustainable Chem. Eng.* **2018**, *6*, 8040−8047.
(26) Kim, J. H.; Gu, M.; Lee, D. H.; Kim, J. H.; Oh, Y. S.; Min, S. H.; Kim, B. S.; Lee, S. Y. Functionalized Nanocellulose-Integrated Heterolayered Nanomats toward Smart Battery Separators. *Nano Lett.* **2016**, *16*, 5533−5541.
(27) Oh, S. Y.; Yoo, D. I.; Shin, Y.; Kim, H. C.; Kim, H. Y.; Chung, Y. S.; et al. Crystalline structure analysis of cellulose treated with sodium hydroxide and carbon dioxide by means of X-ray diffraction and FTIR spectroscopy. *Carbohydr. Res.* **2005**, *340*, 2376−2391.
(28) Kaur, M.; Arshad, M.; Ullah, A. In-Situ Nanoreinforced Green Bionanomaterials from Natural Keratin and Montmorillonite (MMT)/Cellulose Nanocrystals (CNC). *ACS Sustainable Chem. Eng.* **2018**, *6*, 1977−1987.
(29) Arshad, M.; Kaur, M.; Ullah, A. Green Biocomposites from Nanoengineered Hybrid Natural Fiber and Biopolymer. *ACS Sustainable Chem. Eng.* **2016**, *4*, 1785−1793.
(30) Holding, A. J.; Mäkelä, V.; Tolonen, L.; Sixta, H.; Kilpeläinen, I.; King, A. W. T. Solution-state one- and two-dimensional NMR spectroscopy of high-molecular-weight cellulose. *ChemSusChem* **2016**, *9*, 880−892.
(31) Hristea, E. N.; Covaci-Cîmpeanu, I. C.; Ioniţaă, G.; Ioniţaă, P.; Draghici, C.; Caăproiu, M. T.; Balaban, A. T.; et al. Reactions of 2,2-Diphenyl-1-picrylhydrazyl (DPPH) with Two Syringylic Phenols or One Aroxide Derivative. *Eur. J. Org. Chem.* **2009**, *2009*, 626−634.
(32) Ibbett, R. N.; Domvoglou, D.; Fasching, M. Characterisation of the supramolecular structure of chemically and physically modified regenerated cellulosic fibres by means of high-resolution carbon-13 solid-state NMR. *Polymer* **2007**, *48*, 1287−1296.
(33) Guyot, B.; Bosquette, B.; Pina, M.; Graille, J. Esterification of phenolic acids from green coffee with an immobilized lipase from candida antarctica in solvent-free medium. *Biotechnol. Lett.* **1997**, *19*, 529−532.
(34) Reis, B.; Martins, M.; Barreto, B.; Milhazes, N.; Garrido, E. M.; Silva, P.; et al. Structure-property-activity relationship of phenolic acids and derivatives. protocatechuic acid alkyl esters. *J. Agric. Food Chem.* **2010**, *58*, 6986−6993.
(35) Centini, M.; Rossato, M. S.; Sega, A.; Buonocore, A.; Stefanoni, S.; Anselmi, C. New multifunctional surfactants from natural phenolic acids. *J. Agric. Food Chem.* **2012**, *60*, 74−80.
(36) Mazeau, K.; Rivet, A. Wetting the (110) and (100) Surfaces of I beta Cellulose Studied by Molecular Dynamics. *Biomacromolecules* **2008**, *9*, 1352−4.
(37) Wang, J.; Gardner, D. J.; Stark, N. M.; Bousfield, D. W.; Tajvidi, M.; Cai, Z. Moisture and Oxygen Barrier Properties of Cellulose Nanomaterial-Based Films. *ACS Sustainable Chem. Eng.* **2018**, *6*, 49−70.
(38) Fortunati, E.; Peltzer, M.; Armentano, I.; Torre, L.; Jiménez, A.; Kenny, J. M. Effects of modified cellulose nanocrystals on the barrier and migration properties of PLA nano-biocomposites. *Carbohydr. Polym.* **2012**, *90*, 948−956.
(39) Bugnicourt, E.; Cinelli, P.; Alvarez, V.; Lazzeri, A. Polyhydroxyalkanoate (PHA): Review of synthesis, characteristics, processing and potential applications in packaging. *Express Polym. Lett.* **2014**, *8*, 791−808.
(40) Espino-Pérez, E.; Bras, J.; Ducruet, V.; Guinault, A.; Dufresne, A.; Domenek, S. Influence of chemical surface modification of cellulose nanowhiskers on thermal, mechanical, and barrier properties of poly(lactide) based bionanocomposites. *Eur. Polym. J.* **2013**, *49*, 3144−3154.
(41) Khan, R. A.; Beck, S.; Dussault, D.; Salmieri, S.; Bouchard, J.; Lacroix, M. Mechanical and barrier properties of nanocrystalline cellulose reinforced poly(caprolactone) composites: Effect of gamma radiation. *J. Appl. Polym. Sci.* **2013**, *129*, 3038−3046.

DOI: 10.1021/acs.biomac.9b00325
Biomacromolecules 2019, 20, 2105−2114

(42) Khakalo, A.; Filpponen, I.; Rojas, O. J. Protein-mediated interfacial adhesion in composites of cellulose nanofibrils and polylactide: Enhanced toughness towards material development. *Compos. Sci. Technol.* **2018**, *160*, 145.
(43) Yousefi, H.; Nishino, T.; Faezipour, M.; Ebrahimi, G.; Shakeri, A. Direct fabrication of all-cellulose nanocomposite from cellulose microfibers using ionic liquid-based nanowelding. *Biomacromolecules* **2011**, *12*, 4080−4085.
(44) Rojas, O. J. *Cellulose Chemistry and Properties: Fibers, Nanocelluloses and Advanced Materials*; Springer International Publishing, 2016; Chapter 4, pp 115−131.
(45) Hanid, N. A.; Wahit, M. U.; Guo, Q.; Mahmoodian, S.; Soheilmoghaddam, M. Development of regenerated cellulose/halloysites nanocomposites via ionic liquids. *Carbohydr. Polym.* **2014**, *99*, 91−97.
(46) Yang, X.; Berthold, F.; Berglund, L. A. Preserving Cellulose Structure: Delignified Wood Fibers for Paper Structures of High Strength and Transparency. *Biomacromolecules* **2018**, *19*, 3020−3029.
(47) Yang, X.; Berglund, L. A. Water-Based Approach to High-Strength All-Cellulose Material with Optical Transparency. *ACS Sustainable Chem. Eng.* **2018**, *6*, 501−510.
(48) Yang, Q.; Saito, T.; Berglund, L. A.; Isogai, A. Cellulose nanofibrils improve the properties of all-cellulose composites by the nano-reinforcement mechanism and nanofibril-induced crystallization. *Nanoscale* **2015**, *7*, 17957−17963.
(49) Zhang, L.; Ruan, D.; Zhou, J. Structure and Properties of Regenerated Cellulose Films Prepared from Cotton Linters in NaOH/Urea Aqueous Solution. *Ind. Eng. Chem. Res.* **2001**, *40*, 5923−5928.
(50) Toivonen, M. S.; Kurkisuonio, S.; Schacher, F. H.; Hietala, S.; Rojas, O. J.; Ikkala, O. Water-Resistant, Transparent Hybrid Nanopaper by Physical Cross-Linking with Chitosan. *Biomacromolecules* **2015**, *16*, 1062−1071.

DOI: 10.1021/acs.biomac.9b00325
Biomacromolecules 2019, 20, 2105−2114